Academic Education Publishing House

Industry Science and Engineering Vol. 2 No. 12, 2025

Parameter Optimization of Stitch Wires in Four-Span Overlap Sections of High-Speed Railway Catenary

Junqing Chen[1], Xiaolei Hu[2,*], Jinfa Guan[1], Yicheng Xiang[1], Jiayu Fu[1]

[1]*Southwest Jiaotong University, Chengdu, Sichuan, China*

[2]*Beijing–Shanghai High-Speed Railway Co., Beijing, China*

**Corresponding Author*

Abstract: To identify optimal stitch-wire configurations in four-span overlap sections, a finite-element pantograph-catenary model was developed. Four layouts were compared: stitch wires installed throughout the overlap, only at the center pole, none, or throughout with an electric connector. The front pantograph was insensitive to layout, but the rear pantograph showed significant differences. Installing the stitch wire throughout the overlap improved rear-pantograph minimum contact force and reduced its standard deviation, yielding best stability; adding an electric connector had limited effect. Optimal stitch wire tension is 3000 to 3500 N and length 14-18 m (16 m optimal). These findings support structural optimization of high-speed railway overlap sections.

Keywords: Overlap Section; Stitch Wire; Pantograph-Catenary Interaction; Contact Force; Parameter Optimization

1. Introduction

The overlap section is a key structure that enables mechanical sectioning and electrical transition in the catenary system, and it also constitutes the critical region where the pantograph passes smoothly from one contact suspension to the next. Because this region is characterized by the intersection of two contact wires, local geometric discontinuities, variations in structural stiffness, and nonuniform elastic distribution, pantograph-catenary vibration, impact, and contact-force fluctuation tend to concentrate there when trains operate at high speed. The overlap section is therefore widely regarded as the most sensitive zone for current collection and one of the most vulnerable segments of the catenary. The studies by Jiang et al. [1] and Chen [2] both demonstrate that the dynamic behavior of the overlap section has a direct influence on current-collection performance under high-speed operating conditions. In engineering practice, a stitch wire is commonly installed on the working branch to improve the local elasticity distribution, mitigate the hard-point effect, and enhance transition smoothness. Nevertheless, the applicability of this measure and the associated parameter-matching problem in overlap sections with different numbers of spans remain to be clarified. Extensive studies have been carried out on both overlap sections and stitch wires. With respect to overlap sections, Liu and Wu [4] analyzed and calculated the geometrical profile of the overlap section from the perspectives of construction installation and geometric control. Yang et al. [5] performed a finite-element simulation of the dynamic performance of the pantograph-catenary transition region and pointed out that the transition zone is highly sensitive to dynamic response. Guan and Wu [6] conducted a structural optimization study on the four-span overlap section of a high-speed railway catenary. Wu [7] further compared the pantograph-catenary current-collection performance of overlap sections with and without a stitch wire. Deng [8] discussed the influence of the equal-height point in a five-span overlap section on pantograph-catenary performance. Liu [9] has also addressed the optimization of high-speed pantograph-catenary dynamic performance by installing a stitch wire in a four-span overlap section. In the international literature, Hayasaka [10] investigated the incidence and reflection mechanisms of contact-wire vibration waves in overlap sections and proposed suppressing reflected waves to improve current collection. Harèll, Drugge, and Reijm [11] identified the critical weak regions of section overlaps under multiple-pantograph operation. Mei et al. [12] proposed a hybrid simulation method for pantograph-catenary interaction in overlap spans. Gregori et al. [13] compared the dynamic

differences between four-span and five-span overlaps. Jiang et al. [14] employed an optical measurement method to examine the relationship among contact-wire displacement, transition distance, and peak contact force in overlap sections. Yao et al. [15] combined numerical simulation with experimental testing to analyze contact force and uplift response in a four-span overlap section. Song et al. [16] systematically discussed the speed adaptability of overlap sections by considering crossover-point height and steady-arm damping. Regarding stitch wires and dropper dynamics, Li et al. [17] carried out an early study on parameter selection for high-speed catenary systems with elastic chain suspension. Guan, Tian, and Zhang [3] systematically compared the effects of stitch-wire cross-sectional area, tension, and length on pantograph-catenary contact force and support-point uplift, and proposed recommended parameter values for catenary systems designed for 250 km/h and 350 km/h operation. Chen, Peng, and He [18] analyzed the relationship between dropper loading and fatigue life. Chen [19] investigated the dynamic load of integral droppers under the action of a high-speed pantograph. Hu et al. [20] examined the transient dynamic performance of integral droppers in a simple chain suspension catenary. Liu et al. [21] revealed the causes of early failure in integral droppers and proposed optimization strategies. Qin et al. [22] studied the fatigue-failure behavior of integral droppers under impact loading. He and Guo [23], as well as Chen et al. [24], analyzed dropper stress characteristics from the perspectives of load position and stress response, respectively. Wei et al. [25] further linked dropper arrangement optimization with fatigue-life enhancement. Overall, significant progress has been achieved in the study of overlap-section geometry, span configuration, equal-height point arrangement, crossover-point height, as well as stitch-wire tension, length, cross-sectional area, loading characteristics, and fatigue life. However, for four-span overlap sections, existing studies have largely focused on local operating conditions or single-factor analyses, and a systematic investigation into the applicability limits, coordinated parameter design, and speed-grade matching of different stitch-wire configurations is still lacking.

In view of the foregoing research background, this study intends to employ the finite element method to establish a pantograph-catenary coupled model incorporating a four-span overlap section. Under unified boundary conditions and operating scenarios, comparative analyses will be conducted for stitch-wire layouts with different configurations and parameter combinations. Particular attention will be paid to statistical characteristics of pantograph-catenary contact force, contact-wire uplift, loss-of-contact risk, and the dynamic response of the overlap region. On this basis, the effects of stitch-wire configuration, tension, length, and cross-sectional parameters on the dynamic performance of the four-span overlap section will be clarified, thereby providing a basis for performance optimization and offering theoretical support for structural design and maintenance-parameter selection of high-speed railway overlap sections.

2. Simulation Modeling

2.1 Catenary Model

In the pantograph–catenary simulation, the catenary system is represented by masts, support devices, steady arms, and the catenary suspension. Because the masts and support devices primarily provide structural support and experience negligible deformation during pantograph–catenary interaction, they are simplified as fixed points in space in the present model. The steady arm connects the contact wire to the hook ring; owing to its rotational freedom and negligible self-deformation, it is simulated by three-dimensional beam elements, as described in equation (1) (a). Within the catenary suspension, the contact wire, messenger wire, and stitch wire are characterized by relatively large tension, considerable spanwise extent, and pronounced sag, and are therefore discretized using three-dimensional bar elements, as shown in equation (1) (b). The droppers, which suspend the contact wire from the messenger wire and transmit tensile load, may become slack under contact-wire uplift induced by pantograph passage. Accordingly, the droppers are represented by tension-only cable elements without compressive capacity, as given in equation (1) (c).

$$\begin{cases} m_s\ddot{u}_s + k_s u_s = f_s \cdots\cdots\cdots\cdots (a) \\ m_c\ddot{u}_c + (k_c + k_{ct})u_c = f_c \cdots (b) \\ m_d\ddot{u}_d + k_d u_d = f_d \cdots\cdots\cdots (c) \end{cases} \quad (1)$$

where the mass, displacement, and stiffness matrices correspond to the beam, bar, and cable

elements, respectively; for the bar element, both elastic stiffness and geometric stiffness are taken into account.

The governing equations describing the static and dynamic responses of the catenary can thus be written as follows.

$$M\ddot{u} + C\dot{u} + ku + k_{ct}u + k_d u = G + F_{cf} + F_{Tf} \quad (2)$$

where the matrices represent the mass matrix, gravity matrix, and nodal displacement matrix of the catenary, respectively; the Rayleigh damping matrix is formed by proportional combination of the mass and stiffness matrices; the elastic stiffness matrix corresponds to the catenary system; the variable stiffness matrix is associated with the droppers; the geometric stiffness matrix arises from the contact wire, messenger wire, and stitch wire; the vertical load or contact-force matrix acts as the external excitation; and the nodal tension matrix is imposed at both ends of the catenary.

A crucial step in establishing the initial static configuration of the catenary is the accurate determination of the messenger-wire nodal coordinates. This objective is achieved through the following iterative procedure.

Place the nodes of the contact wire, messenger wire, droppers, steady arms, and other components at their prescribed spatial positions, connect them to form the corresponding beam, bar, and cable elements, and impose the relevant boundary conditions. The messenger wire between two fixed points is initially assumed to be straight.

1. Constrain all six degrees of freedom at each messenger-wire node.
2. Calculate the axial force in each dropper under the current configuration.
3. Following Step 1, construct a reduced model containing only the straight messenger-wire elements and their associated boundary conditions.
4. Apply the dropper axial forces obtained in Step 2 as concentrated loads at the corresponding messenger-wire nodes.
5. Determine the static equilibrium position of the messenger wire.
6. Reconstruct the model according to Step 1 and update the messenger-wire nodal coordinates using the static displacements obtained in the preceding step.
7. Solve for the static equilibrium of the catenary suspension, and record the messenger-wire position together with the contact-wire height.
8. Repeat Steps 6 and 7 until the contact-wire height satisfies the prescribed accuracy requirement.

The static equilibrium configuration obtained by the above procedure is adopted as the initial equilibrium state of the catenary, as shown in Figure 1.

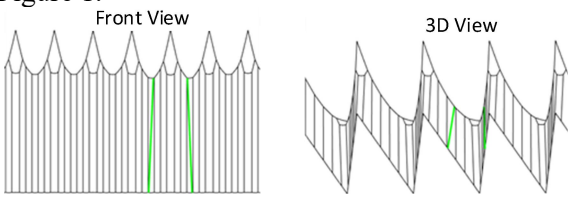

Figure 1. Initial Equilibrium Configuration of the Catenary System

2.2 Pantograph and Pantograph–Catenary Contact Model

The pantograph is represented by an equivalent three-mass–spring–damper lumped-parameter model, and its governing differential equations are expressed as follows.

$$\begin{cases} m_1\ddot{y}_1(t) + c_1(\dot{y}_1(t) - \dot{y}_2(t)) + k_1(y_1(t) - y_2(t)) + f_c(t) = 0 \\ m_2\ddot{y}_2(t) + c_1(\dot{y}_2(t) - \dot{y}_1(t)) + c_2(\dot{y}_2(t) - \dot{y}_3(t)) + k_1(y_2(t) - y_1(t)) + k_2(y_2(t) - y_3(t)) = 0 \\ m_3\ddot{y}_3(t) + c_2(\dot{y}_3(t) - \dot{y}_2(t)) + c_3\dot{y}_3(t) + k_2(y_3(t) - y_2(t)) + k_3 y_3(t) - f_0 = 0 \end{cases} \quad (3)$$

where the mass terms denote the equivalent masses of the panhead, upper frame, and lower arm, respectively; the damping terms represent the equivalent damping coefficients of these three components; the stiffness terms denote their equivalent stiffnesses; the pantograph–catenary contact force and the static contact force are represented separately; and the coordinate variables correspond to the equivalent coordinates of the panhead, upper frame, and lower arm at time t.

In the present study, pantograph–catenary interaction is formulated as a sliding-contact problem. Time integration is carried out using the Newmark-β method, and the pantograph advances according to the discrete time step. The contact constraint is enforced by a penalty-function approach. More specifically, contact or separation is identified from the vertical penetration displacement between the contact-wire element and the pantograph mass point: when u(t) > 0, the pantograph remains in contact with the catenary; otherwise, separation occurs. The contact force is therefore given by:

$$f_c(t) = \begin{cases} k_c u(t) & u(t) \geq 0 \\ 0 & u(t) < 0 \end{cases} \quad (4)$$

where t denotes time and k_c denotes the contact stiffness.

By integrating the catenary model, the pantograph model, and the pantograph–catenary contact model, a simulation framework for the dynamic behavior of pantograph–catenary interaction is established, as illustrated in Figure 2.

2.3 Evaluation Criteria for Pantograph–Catenary Dynamic Performance

According to TB 10621-2014, Code for Design of High-Speed Railway, the extrema and standard deviation of contact force are adopted as the evaluation indices for pantograph–catenary dynamic performance, as summarized in Table 1.

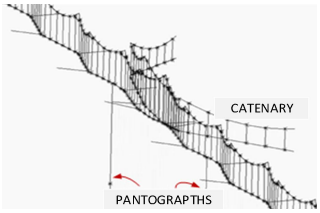

Figure 2. Three-Dimensional Simulation Model Of Pantograph–Catenary Interaction

Table 1. Contact Force

Speed/ km·h^{-1}	Contact force / N			
	Mean	Standard deviation	Maximum	Minimum
250	≤130	$< 0.3F_m$	≤250	>0
300	≤150		≤250	>0
350	≤180		≤350	>0

As an important index for assessing current-collection quality, the standard deviation of contact force reflects the fluctuation amplitude of the interaction force. A smaller standard deviation indicates weaker fluctuation of contact force and, consequently, superior dynamic performance of the pantograph–catenary system. Therefore, reducing the standard deviation of contact force constitutes a key objective in dynamic-performance optimization.

The standard deviation of contact force, σ, is defined as

$$\sigma = \sqrt{\frac{\sum_{i=1}^{n} (F_i - F_m)^2}{n-1}} \quad (5)$$

where n is the number of sampled contact-force data points within the analysis section, and F_i represents the i-th sampled contact force.

2.4 Model Parameters

Using the parameter set of the Beijing–Shanghai High-Speed Railway as a reference, a finite element model of a five-span transition overlap section is established on the basis of the existing four-span flexible catenary transition overlap and the standard technical specifications. Subsequently, the stitch-wire parameters and geometric parameters are optimized to enhance the dynamic current-collection performance of the pantograph–catenary system and to improve the operational safety and reliability of the catenary.

The existing catenary model is established using pantograph-catenary simulation model, as shown in Figure 3.

The detailed parameters of the existing catenary are presented in Table 2.

The pantograph is simplified as a three-mass model, and the corresponding parameters are listed inTable 3.

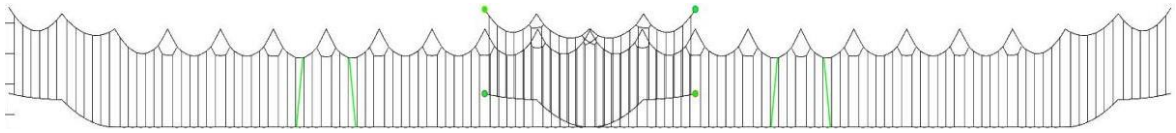

Figure 3. Finite Element Model of the Four-Span Transition Overlap Section in the Flexible Catenary

Table 2. Main Parameters of the 350 km/h Catenary Model

Item		Parameter	Item		Parameter
Span length		50 m	System height		1.6 m
Nominal height		5.3 m	Stagger		±0.25 m
Contact wire	Tension	28500 kN	Total length		650×2 m
	Linear density	1.347 kg/m	Maximum pre-sag of contact wire		0
	Stiffness	N/m	Number of droppers per span		6
Messenger wire	Tension	21 kN	Element length		0.1 m
	Linear density	1.059 kg/m	Dropper	Linear density	0.11 kg/m
	Stiffness	N/m		Stiffness	N/m
Dropper spacing within one span		5 m / 8 m / 8 m / 8 m / 8 m / 8 m / 5 m			

Table 3. Parameters of the Three-Mass Pantograph Model

Type	m_3(kg)	m_2(kg)	m_1(kg)	k_3 (N/m)	k_2 (N/m)	k_1 (N/m)	c_3 (Ns/m)	c_2 (Ns/m)	c_1 (Ns/m)
CX-G1	5	9.98	9	6000	8971	0.5	5	5	350

3. Simulation Analysis

Based on the dynamic model of a four-span overlap section, a comparative analysis is conducted with respect to three factors: the arrangement of stitch wires on the working and non-working branches, the stitch wire tension, and the stitch wire length. The evaluation indices include the contact-force time history, maximum value, minimum value, mean value, standard deviation, and 0.3Fm-σ. While preserving the completeness of the original figures and tables, the layout of the figures has been reorganized to facilitate direct incorporation into the manuscript.

3.1 Analysis of Stitch Wire Arrangements on the Working and Non-Working Branches

The pantograph–catenary dynamic performance under four stitch wire arrangement conditions is analyzed as follows:

a) Condition 1: Stitch wires are installed throughout the entire overlap section.

b) Condition 2: Stitch wires are installed only at the central mast.

c) Condition 3: No stitch wire is installed in the overlap section.

d) Condition 4: Stitch wires and a longitudinal electrical connector are installed throughout the entire overlap section.

First, different stitch wire arrangement schemes on the working and non-working branches are compared. Figure 4 presents the static models of the four transition configurations, and Figure 5 shows the corresponding dynamic contact-force curves at 350 km/h. Table 4 and Figure 6 summarize the extreme values and standard deviations. These figures and tables provide a systematic basis for comparing the effects of different arrangements on the current collection quality of the front and rear pantographs.

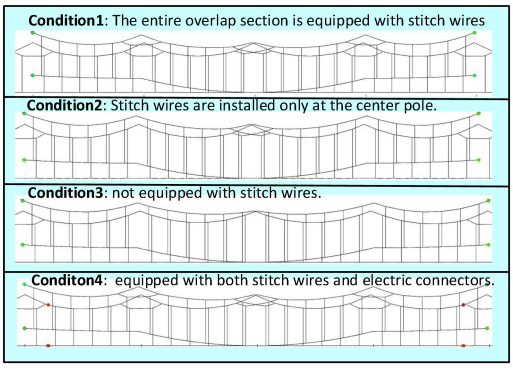

Figure 4. Static Models of Different Transition Configurations in the Four-Span Overlap Section.

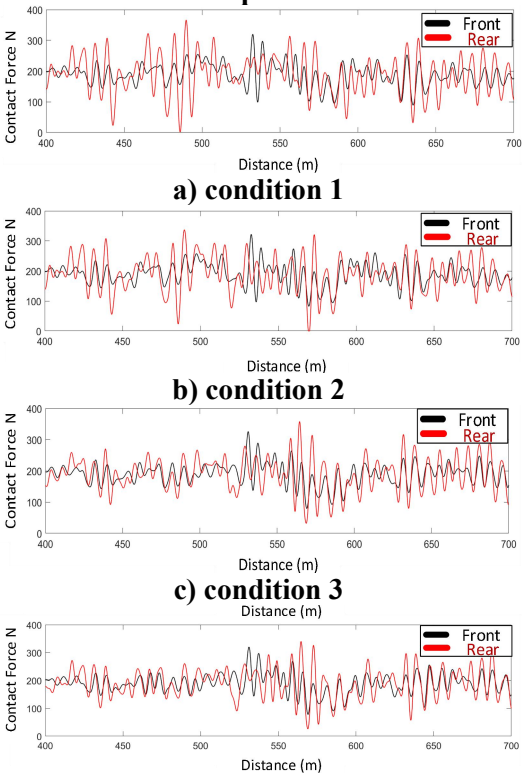

Figure 5. Dynamic Contact Force under Different Stitch Wire Arrangements on the Working and Non-Working Branches.

Table 4. Statistics of Contact Force under Different Stitch Wire Arrangements on the Working and Non-Working Branches

Transition configuration	Panto.	Max. Contact force/N	Min. Contact force/N	Mean contact force(Fm)/N	Std. dev.(σ)/N	0.3Fm-σ/N
Stitch wires throughout the overlap section	Lead.	326	79.45	189.35	33.68	23.125
Stitch wires only at the central mast	Lead.	322.03	82.31	188.72	36.29	20.326
No stitch wire	Lead.	320.04	89	188.61	35.72	20.863
Stitch wires + electrical connector	Lead.	320.19	77.77	188.91	34.64	22.033
Stitch wires throughout the overlap section	Trail.	358.09	31.94	189.84	52.17	4.782
Stitch wires only at the central mast	Trail.	337.13	0	189.49	56.99	-0.143
No stitch wire	Trail.	366.15	1.33	189.06	61.4	-4.682
Stitch wires + electrical connector	Trail.	340	25.96	189.51	51.69	5.163

As shown in Table 4 and Figure 6, the mean contact force of the front pantograph remains within 188.61 – 189.35 N for all four arrangement schemes, with only small differences in the maximum value and standard deviation, indicating that the front pantograph is relatively insensitive to the arrangement configuration. In contrast, the response of the rear pantograph is much more pronounced. When stitch wires are installed only at the central mast or omitted altogether, the minimum contact force decreases to 0 N and 1.33 N, respectively, and the values of 0.3Fm- σ are -0.143 N and -4.682 N, indicating an increased risk of loss of contact. When stitch wires are installed throughout the entire overlap section, the minimum contact force of the rear pantograph increases to 31.94 N and the standard deviation decreases to 52.17 N, yielding better overall performance than the previous two schemes. After a longitudinal electrical connector is further added, the statistical indices of both the front and rear pantographs change only slightly, suggesting that the electrical connector has a limited influence on the pantograph – catenary dynamic characteristics, although the contact-force fluctuation increases slightly. Therefore, the subsequent parametric analysis is carried out based on the transition configuration in which stitch wires are installed throughout the entire overlap section.

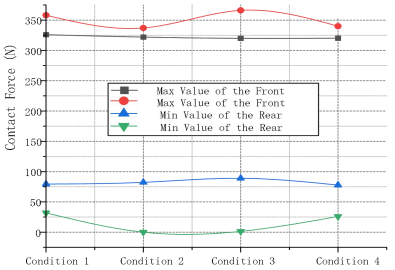

a) Extreme Values

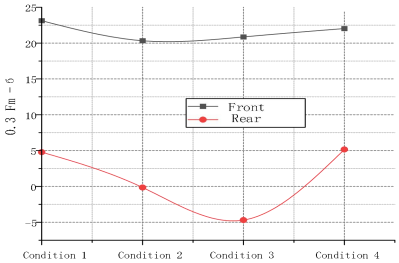

b) Standard Deviation

Figure 6. Extreme Values and Standard Deviations of Contact Force under Different Transition Configurations.

3.2 Analysis of Stitch Wire Tension

Figure 7 presents the contact-force time histories for tensions ranging from 2000 to 10000 N, and Table 5 lists the corresponding statistical results. By comparing the changes in the extreme values and dispersion indices at different tension levels, a reasonable range of stitch wire tension can be identified.

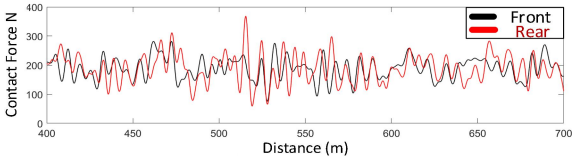

a) 2000 N

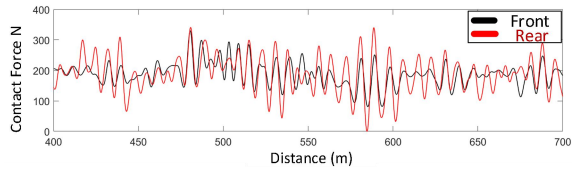

b) 3000 N

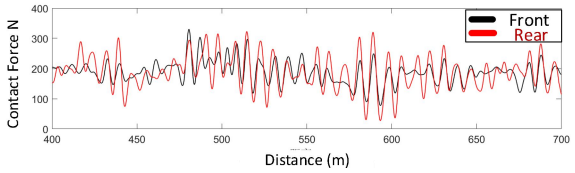

c) 3500 N

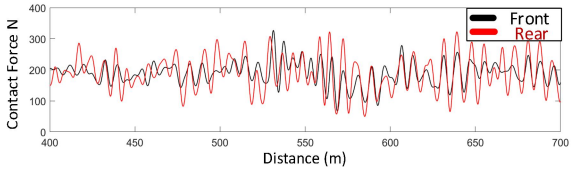

d) 4000 N

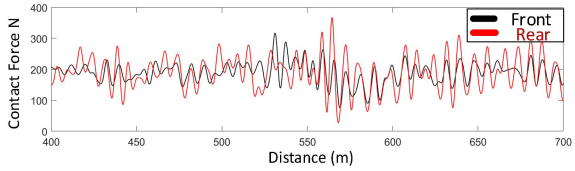

e) 6000 N

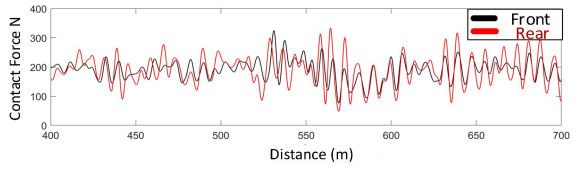

f) 10000 N

Figure 7. Dynamic Contact Force under Different Stitch Wire Tensions.

As shown in Table 5, the mean contact force of the front pantograph remains approximately 189 N for all cases, while the standard deviation is mainly distributed within 33.30-38.16 N, indicating that the front pantograph is not sensitive to tension variation. The difference in the rear pantograph is more evident. When the tension is 3000 N, the rear pantograph exhibits

the lowest standard deviation of 50.55 N. At 3500 N, the standard deviation is 52.17 N, while the minimum contact force remains 31.94 N. When the tension increases to 4000 N, the maximum contact force reaches 367.59 N and the minimum contact force decreases to 27.13 N, indicating a marked increase in fluctuation amplitude. When the tension is further increased to 10000 N, the minimum contact force drops to 0 N and 0.3Fm- σ becomes -2.045 N, which is unfavorable for stable current collection. Considering both the extreme-value and dispersion indices, the stitch wire tension should preferably be controlled within the range of 3000 – 3500 N.

3.3 Analysis of Stitch Wire Length

After the tension range is determined, the influence of stitch wire length on current collection quality is further examined. Table 6 and Figure 8 present the corresponding statistical results. By comparing the maximum value, minimum value, and standard deviation at different lengths, a preferable range of geometric parameters can be further identified.

As shown in Table 6, as the stitch wire length increases, the mean contact force of the front pantograph changes only slightly, whereas the standard deviation and extreme values exhibit certain differences. In particular, under the 16 m and 18 m conditions, the standard deviation of the front pantograph is 33.09 N and 33.68 N, respectively, and the corresponding maximum and minimum contact forces also remain within a reasonable range. For the rear pantograph, as the length increases from 12 m to 24 m, the maximum contact force generally increases whereas the minimum contact force generally decreases. In particular, at 22 m and 24 m, the minimum contact force is only 13.81 N and 21.01 N, respectively, while the standard deviation increases to 56.87 N and 58.04 N, indicating a clear deterioration in dynamic performance. Considering the variations in the extreme values and standard deviation shown in Figure 8, the preferable length range is 14–18 m, among which 16 m provides a better balance between a relatively low standard deviation and relatively stable extreme values, and can therefore be recommended.

In summary, for a four-span overlap section, the arrangement in which stitch wires are installed throughout the entire overlap section provides the best current collection stability for the rear pantograph. On this basis, a stitch wire tension of 3000–3500 N and a length of 16 m are recommended. This parameter combination can provide a basis for subsequent structural optimization and engineering application.

Table 5. Statistics of Contact Force under Different Stitch Wire Arrangements on the Working and Non-Working Branches

Tension/N	Panto.	Max. Contact force/N	Min. Contact force/N	Mean contact force (Fm)/N	Std. dev. (σ) / N	0.3Fm-σ/N
2000	Lead.	329.54	77.59	189.28	34.47	22.314
3000	Lead.	324.47	75.45	189.36	34.42	22.388
3500	Lead.	326	79.45	189.35	33.68	23.125
4000	Lead.	317.02	75.6	188.97	33.3	23.391
6000	Lead.	327.1	66.57	189.01	36.01	20.693
8000	Lead.	330.06	77.35	187.58	36.9	19.374
10000	Lead.	330.51	80.75	187.63	38.16	18.129
2000	Trail.	364.87	15.71	189.89	54.29	2.677
3000	Trail.	332.68	47.9	189.83	50.55	6.399
3500	Trail.	358.09	31.94	189.84	52.17	4.782
4000	Trail.	367.59	27.13	189.48	53.22	3.624
6000	Trail.	322.4	49.4	189.47	55.84	1.001
8000	Trail.	332.82	27.24	188.26	54.3	2.178
10000	Trail.	341.2	0	188.25	58.52	-2.045

Table 6. Statistics of Contact Force under Different Stitch Wire Lengths

Length/m	Panto.	Max. Contact force/N	Min. Contact force/N	Mean contact force (Fm)/N	Std. dev. (σ)/N	0.3Fm-σ/N
12	Lead.	338.37	78.8	188.58	35.09	21.484
14	Lead.	347.14	65.56	188.75	34.64	21.985
16	Lead.	321.28	72.34	188.87	33.09	23.571
18	Lead.	326	79.45	189.35	33.68	23.125
20	Lead.	332.03	74.94	189	33.88	22.82
22	Lead.	334.61	89.76	189.04	33.65	23.062
24	Lead.	317.17	92.49	189.05	31.64	25.075
12	Trail.	309.37	62.84	188.8	49.57	7.07

14	Trail.	316.36	48.93	189.13	50.92	5.819
16	Trail.	318.78	33.74	189.28	53.23	3.554
18	Trail.	358.09	31.94	189.84	52.17	4.782
20	Trail.	370.72	28.56	189.63	56.47	0.419
22	Trail.	374.1	13.81	189.7	56.87	0.04
24	Trail.	359.57	21.01	189.54	58.04	-1.178

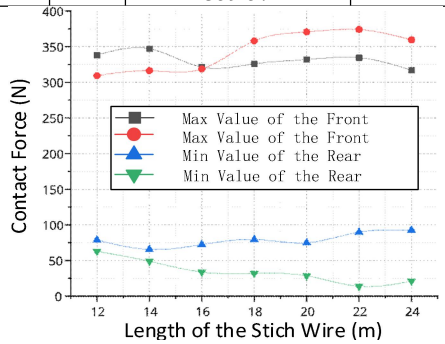

a) Extreme values

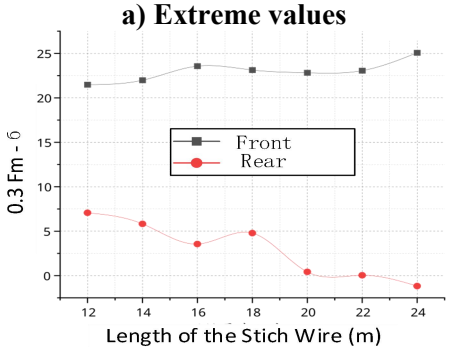

b) Standard deviation

Figure 8. Extreme Values and Standard Deviations of Contact Force under Different Stitch Wire Lengths.

4. Conclusions

(1) Simulation results demonstrate that the stitch wire parameters significantly affect the pantograph–catenary dynamic performance in a four-span overlap section. Among the investigated arrangement schemes, installing stitch wires throughout the entire overlap section yields the best overall performance. This configuration has only a limited influence on the front pantograph, but it effectively increases the minimum contact force and reduces the contact force standard deviation of the rear pantograph, thereby decreasing the risk of loss of contact. In contrast, when stitch wires are installed only at the central mast, or are not installed at all, the rear pantograph exhibits a markedly lower minimum contact force and poorer current collection stability, while the improvement obtained by adding an electrical connection remains limited.

(2) In terms of tension, the preferable range is 3000-3500 N. A tension of 3000 N leads to the smallest fluctuation in the contact force of the rear pantograph, whereas 3500 N provides a better balance between a relatively low standard deviation and a relatively high minimum contact force. When the tension exceeds this range, both contact force fluctuation and the risk of loss of contact increase.

(3) In terms of length, the preferable range is 14-18 m, among which 16 m provides the most balanced performance with respect to the extreme values and standard deviations of the contact force for both the front and rear pantographs, indicating a more stable dynamic response.

Overall, for a four-span overlap section, the recommended parameter combination is stitch wires installed throughout the entire overlap section, with a tension of 3000-3500 N and a length of 16 m. This combination is beneficial for improving current collection stability and enhancing operational safety.

Acknowledgments

This work was supported by: The Science and Technology Research Project of Beijing–Shanghai High-Speed Railway Co., Ltd. (Project Title: Research on Maintenance Strategies of Existing High-Speed Railway Overhead Contact Systems Based on Model Reconstruction; Number: Research of JINGHU -2024-21). (Corresponding author: Hu Xiaolei.)

References

[1] Jiang Hongpeng, Xu Yan, Liu Zhendong, et al. Study on the dynamic behavior of a catenary overlap section under dropper failure[J]. Electric Drive for Locomotives, 2024(3): 182-189.

[2] Chen Wei. Influence of overlap-section configuration on pantograph-catenary current-collection performance in high-speed railways[J]. Journal of Railway Engineering Society, 2025, 42(8): 82-86.

[3] Guan Jinfa, Tian Zhijun, Zhang Xuewu. Influence of stitch-wire parameters in the catenary on pantograph-catenary dynamic performance[J]. Journal of Southwest Jiaotong University, 2021, 56(3): 659-665.

[4] Liu Yang, Wu Nan. Analysis and calculation of the geometrical profile of catenary

overlap sections[J]. Journal of Railway Engineering Society, 2012, 29(5): 49-53.
[5] Yang Yi, Zhou Ning, Li Ruiping, et al. Finite-element simulation analysis of the dynamic performance of pantograph-catenary transition sections[J]. Journal of Vibration and Shock, 2016, 35(18): 71-75.
[6] Guan Jinfa, Wu Jiqin. Structural optimization of a four-span overlap section in high-speed railway catenary[J]. Railway Standard Design, 2017, 61(7): 159-164.
[7] Wu Yafei. Analysis of the influence of stitch wires on pantograph-catenary current collection at catenary overlap sections[J]. Railway Standard Design, 2020, 64(9): 158-161.
[8] Deng Hong. Influence of the equal-height point in a five-span overlap section on pantograph-catenary performance[J]. Journal of Railway Engineering Society, 2023, 40(12): 61-65.
[9] Liu Dayong. Optimization of high-speed pantograph-catenary dynamic performance based on a stitch wire installed in a four-span overlap section[J]. Journal of Railway Science and Engineering, 2025, 22(4): 1769-1777.
[10] Hayasaka T. Effect of Reduced Reflective Wave Propagation on Overhead Contact Lines in Overlap Section[J]. Quarterly Report of RTRI, 2004, 45(2): 68-73.
[11] Harèll P, Drugge L, Reijm M. Study of Critical Sections in Catenary Systems During Multiple Pantograph Operation[J]. Proceedings of the Institution of Mechanical Engineers, Part F: Journal of Rail and Rapid Transit, 2005, 219(4): 203-211.
[12] Mei G, Zhang W, Zhao H, et al. A Hybrid Method to Simulate the Interaction of Pantograph and Catenary on Overlap Span[J]. Vehicle System Dynamics, 2006, 44(sup1): 571-580.
[13] Gregori S, Gil J, Tur M, et al. Analysis of the Overlap Section in a High-Speed Railway Catenary by Means of Numerical Simulations[J]. Engineering Structures, 2020, 221: 110963.
[14] Jiang T, Frøseth G T, Nåvik P, et al. Assessment of Pantograph-Catenary Interaction in a Railway Overlap Section via a Novel Optical-Based Method[J]. Mechanism and Machine Theory, 2022, 177: 105045.
[15] Yao Y, Yang Z, Wang J, et al. Analysis of Contact Force and Uplift of Pantograph-Catenary System in Overlap Section Based on Numerical Simulations and Experimental Tests[J]. Vehicle System Dynamics, 2023, 61(10): 2492-2515.
[16] Song Y, Rønnquist A, Jiang T, et al. Railway Pantograph-Catenary Interaction Performance in an Overlap Section: Modelling, Validation and Analysis[J]. Journal of Sound and Vibration, 2023, 548: 117506.
[17] Li Wenhao, Cui Xiaoyu, Chen Weirong. Study on parameter selection for high-speed catenary systems with elastic chain suspension[J]. Journal of Railway Engineering Society, 2009, 26(8): 82-87.
[18] Chen L, Peng P, He F. Fatigue Life Analysis of Dropper Used in Pantograph-Catenary System of High-Speed Railway[J]. Advances in Mechanical Engineering, 2018, 10(5): 1-10.
[19] Chen L. Study on Dynamic Force of Integral Dropper of Catenary under Action of High-Speed Pantograph[J]. China Railway Science, 2018, 39(3): 86-92.
[20] Hu Y, Huang P, Ma R, et al. A Study on the Transient Dynamic Performance of Integral Dropper of Simple Chain Suspension Catenary[J]. Journal of Vibration and Shock, 2021, 40(8): 131-136.
[21] Liu X Y, Peng J F, Tan D Q, et al. Failure Analysis and Optimization of Integral Droppers Used in High Speed Railway Catenary System[J]. Engineering Failure Analysis, 2018, 91: 496-506.
[22] Qin Y, Xiao S, Lu L, et al. Fatigue Failure of Integral Droppers of High-Speed Railway Catenary under Impact Load[J]. Engineering Failure Analysis, 2022, 134: 106086.
[23] He F, Guo D D. The Effects of Load Location on Dropper Stress in a Catenary System for a High-Speed Railway[J]. Mathematical Problems in Engineering, 2020, 2020: 1-10.
[24] Chen L, Sun J, Pan L, et al. Analysis of Dropper Stress in a Catenary System for a High-Speed Railway[J]. Mathematical Problems in Engineering, 2022, 2022: 1-7.
[25] Wei W, Zhang H, Xia L, et al. Fatigue Life Enhancement of Catenary Droppers for High-Speed Railways Based on Arrangement Optimization[J]. Engineering Failure Analysis, 2024, 163: 108480.